Electronic Supplementary Information (11 Pages, 12 Figures):

Effects of Ice and Supercooled Water on the Metastability of Methane Hydrate: DSC Analysis and MD Simulations

Ronghui Sun,[a] Zhen Fan,[b] Kehan Li,[a] Mingjun Yang,*[a] and Yongchen Song.*[a]

a. Key Laboratory of Ocean Energy Utilization and Energy Conservation of Ministry of Education, Dalian University of Technology, Dalian, Liaoning, 116024, China.
b. WestCHEM, School of Chemistry, Joseph Black Building, University of Glasgow, Glasgow, G12 8QQ, United Kingdom.

* Corresponding Authors. Email: yangmj@dlut.edu.cn; songyc@dlut.edu.cn.

1. Formation Processes of MH-ice-gas and MH-SW-gas Samples in the Porous Medium

In this study, fine quartz particles were employed to pack the porous medium (as to increase the gas-water interface area and mimic the porous nature of MH sediments) for the formation of MH-ice-gas and MH-SW-gas samples, respectively, as described in Section 2.2.
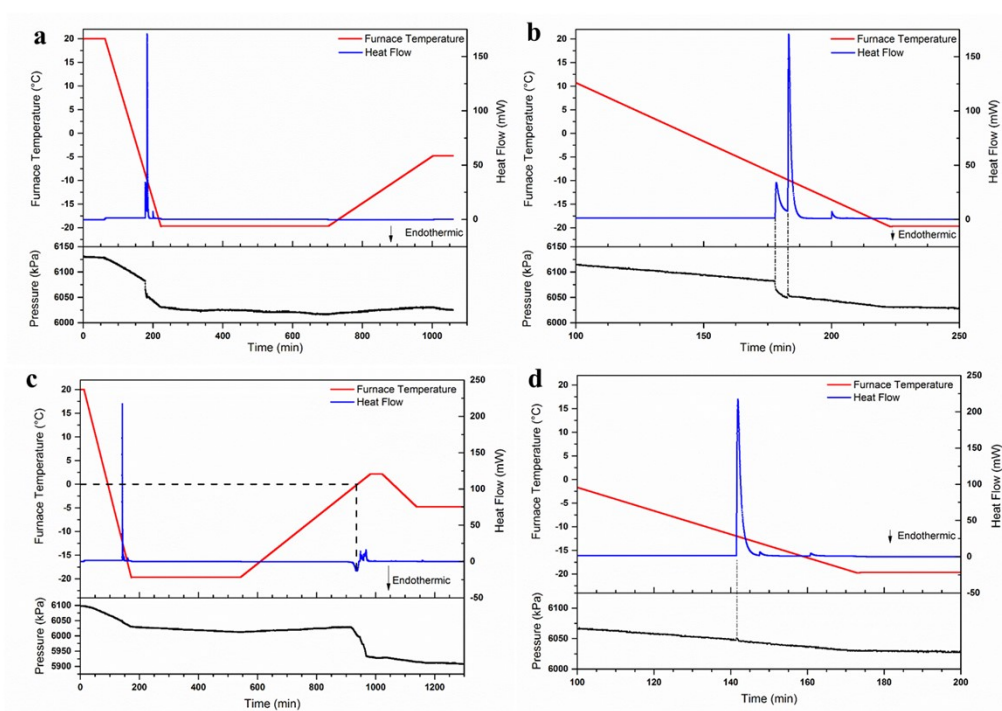

Figure S1. (a) The DSC heat flow curve and P-T evolutions with time for the typical synthesis of MH-ice-gas sample in the porous medium, **(b)** The zoomed-in plot at 100 – 250 min corresponding (a), **(c)** The DSC heat flow curve and P-T evolutions with time for the typical synthesis of MH-SW-gas sample in the porous medium, and **(d)** The zoomed-in plot at 100 – 200 min corresponding to (c).

The representative DSC heat flow curves and P-T evolutions with time for a typical formation process of the MH-ice-gas sample were illustrated in **Figures S1a,b**. The pressure decreased when the temperature dropped from 20 to -20 °C, during which sharp exothermic peaks in the DSC curves emerged, indicating the formation of MH and ice (due to the exothermic properties of these phase changes). A slight pressure increase could be identified in **Figure S1b**, corresponding to the onset of the most intensive exothermic peak (*i.e.* the 2nd peak in **Figure S1b**). Since the exothermic process of MH formation would consume large amounts of methane gas (as indicated by the first exothermic peak in **Figure S1b**), the most intensive exothermic peak is attributed to the formation of ice. The rest exothermic peaks were mainly caused by the formation of MH in the porous medium, agreeing well with the pressure evolutions in the sample cavity. Several peaks could be seen due to the formation of MH, indicating that the formation of MH did not exhibit one-

step characteristics. For the MH-ice-gas samples, no peaks in the DSC heat flow curves can be observed with the pressure remaining relatively steady when the temperature dwelled at -20 °C and subsequently increased and stabilized at -5 °C. This confirmed the stability of the as-formed MH-ice-gas sample without any obvious non-equilibrium phase changes.

Figures S1c,d show the representative DSC heat flow curves and P-T evolutions with time for the typical synthesis of MH-SW-gas samples. The programmed temperature decrease and dwelling processes were kept the same with **Figures S1a,b**, and similar MH formation phenomena were observed. Then the temperature increased to 5 °C with a ramp rate of 0.05 °C/min to melt the as-formed ice (*i.e.* the endothermic peak at 0 °C in **Figure S1c**). This endothermic peak was closely followed by a couple of exothermic peaks of MH formation (*i.e.* with the further rapid pressure drops in **Figure S1c**), which agreed well with published studies that the formation of MH could be promoted during the melting of ice[1]. Moreover, relatively more MH could be formed in the MH-SW-gas sample than in the MH-ice-gas system, attributed to the further pressure drop in **Figure S1c**. Taking these two typical MH formation processes into account (**Figure S1**), ice generations in the sample cell happened at relatively low temperatures (< -10 °C) with the sub-cooling degree as reported in literature[2]. No obvious peaks emerged in the DSC curve when the temperature decreased to -5 °C. The results confirmed that the MH-ice-gas and MH-SW-gas samples can be reproducibly synthesized and stabilized by the temperature-controlling routes in this study (as described in Section 2.2).

2. Supplementary DSC Experimental Results for the Decomposition Processes of MH-ice-gas and MH-SW-gas Samples in the Porous Medium
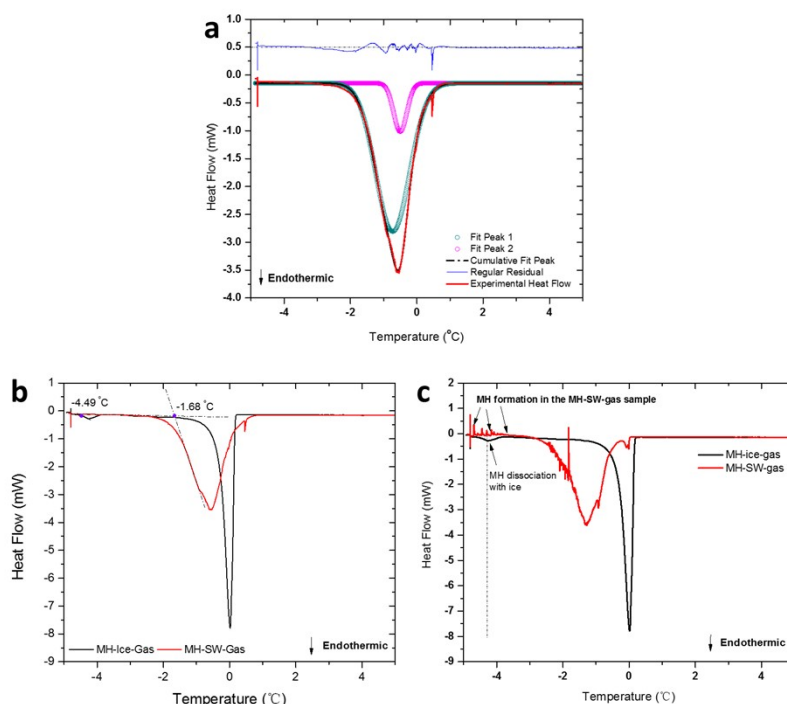

Figure S2. (a) The plot of Gaussian profile fitting against experimental DSC heat flow curves with respect to temperature for the MH-SW-gas sample (case 4, Table 1); and **(b,c)** Comparisons of the DSC heat flow curves against temperature for MH-ice-gas and MH-SW-gas samples in cases 1&4 and cases 3&5, respectively (Table 1).
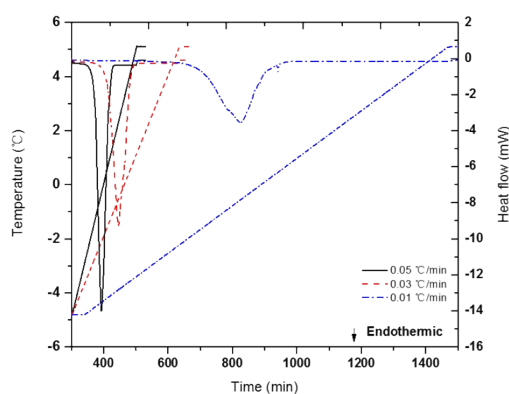
Figure S3. Evolutions of the DSC heat flow and temperature with respect to time under different heating ramp rates (MH-SW-gas samples, initial pressure of ~ 2.20 MPa; cases 4,7&8, Table 1).

The absorbed heat during MH dissociation was calculated by integrating the areas of endothermic heat-flow peaks in **Figure S3**, which were -23.1246, -23.0478, and -25.6974 J for a ramp rate of 0.05, 0.03, and 0.01 °C/min, respectively.
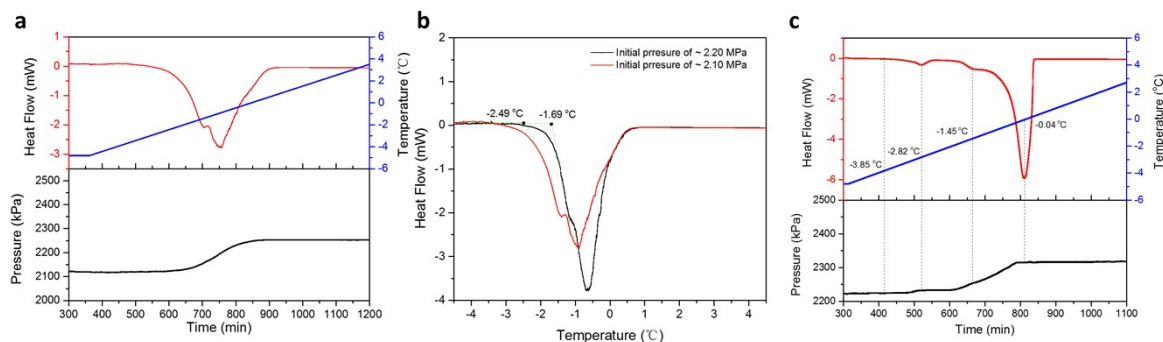
Figure S4. Repeated experiments demonstrating the reproducibility of DSC results in this work. Showing: **(a**, **b)** two repeated DSC measurements of MH-SW-gas samples; and **(c)** a repeated DSC measurement of the MH-ice-gas sample.

3. Molecular Dynamics (MD) Simulations - Validations and Supplementary Results
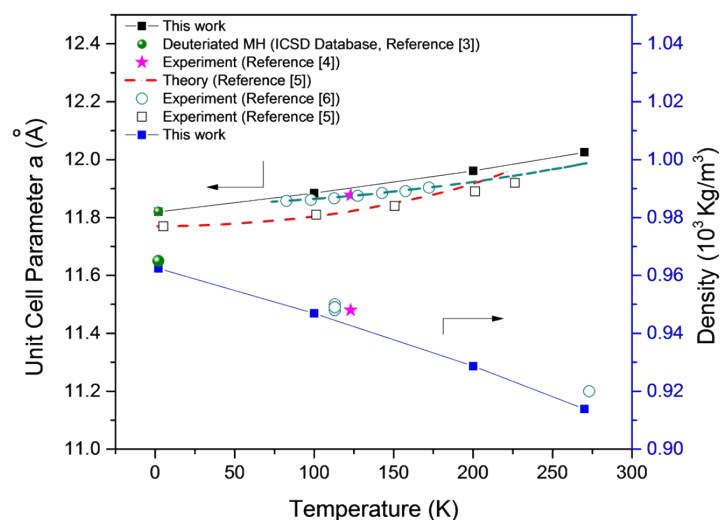
3.1 MD Simulations of 2×2×2 MH unit cells
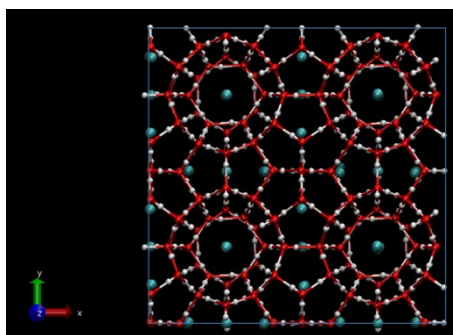
Figure S5. The crystallographic structure of MH from the MD simulations at 2 K and 1 bar for 2 ns, showing stable and crystalline 2×2×2 MH unit cells with no abnormal atomic and molecular positions. (Red sphere: Oxygen atom, Silver sphere: Hydrogen atom, Cyan sphere: Methane molecule, and Red bond: Oxygen bond.)

Table S1. Validations of important physical parameters of MH from MD simulation results in this study (T = 2 K and P = 1 bar) with the equivalent values from the database[3].

Parameter	Literature Study from the ICSD Database[3]	MD Simulation Results in This Study
Temperature (K)	2	2
Pressure (Bar)	1	1
Unit Cell Parameter *a* /	11.821	11.820
Density / 10^3 kg/m³	0.956 [a]	0.9624
Thermal Displacement of Methane / [b]	0.1	0.09312 (in the $5^{12}6^2$ cages) 0.04054 (in the 5^{12} cages)

[a]. Value converted from the density of the equivalent deuterated methane hydrate (formed by CD_4 and D_2O) from the database. [b]. Mean square displacement values were used for the MD simulations.

Figure S6. The unit cell parameter and density of MH at different temperatures from the MD simulations results in this study and reported in the literature[3-6].
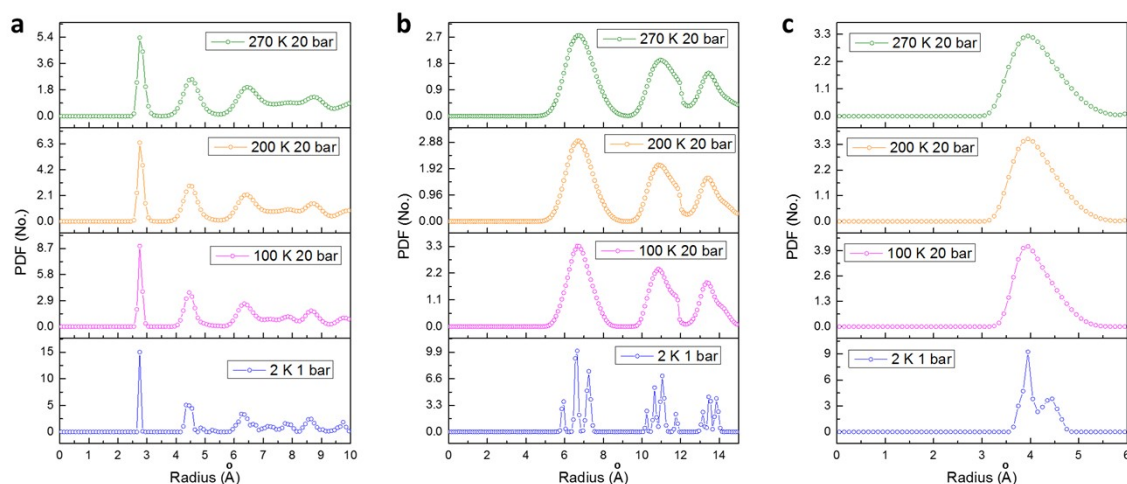

Figure S7. Radial pair distribution functions of the **(a)** O – O, **(b)** C – C, and **(c)** O – C pairs at different temperatures from the MD simulation results in this study.

The widely used radial pair distribution function (PDF) analysis was employed to characterize the atomic-scale structure of MH at different temperatures as shown in **Figure S7** and to characterize the local structure & bonding information of the decomposed water molecules (**Figure 8b**)[7]. Generally, the reduced atomic PDF describes the number of atoms located in a spherical shell (of unit thickness) at a distance of r from a reference atom:[7]

$$G(r) = 4\pi r[\rho(r) - \rho_0] \qquad \text{(Equation S1)}$$

Here, $\rho(r)$ and ρ_0 are the local and average atomic number densities, respectively. Distinct

pairs of atoms and their distances can be signaled through the peak positions and peak profile.[7] **Figure S7** confirmed sharp PDF peaks of O – O, C – C, O – C pairs at 2 K 1bar, indicating the rigid and less-distorted crystallographic structure with discrete host-host and host-guest distances. Moreover, it can be seen that the dynamics features (*i.e.* the movements of atoms and molecules) increased with temperature, indicating distorted structures of MH.
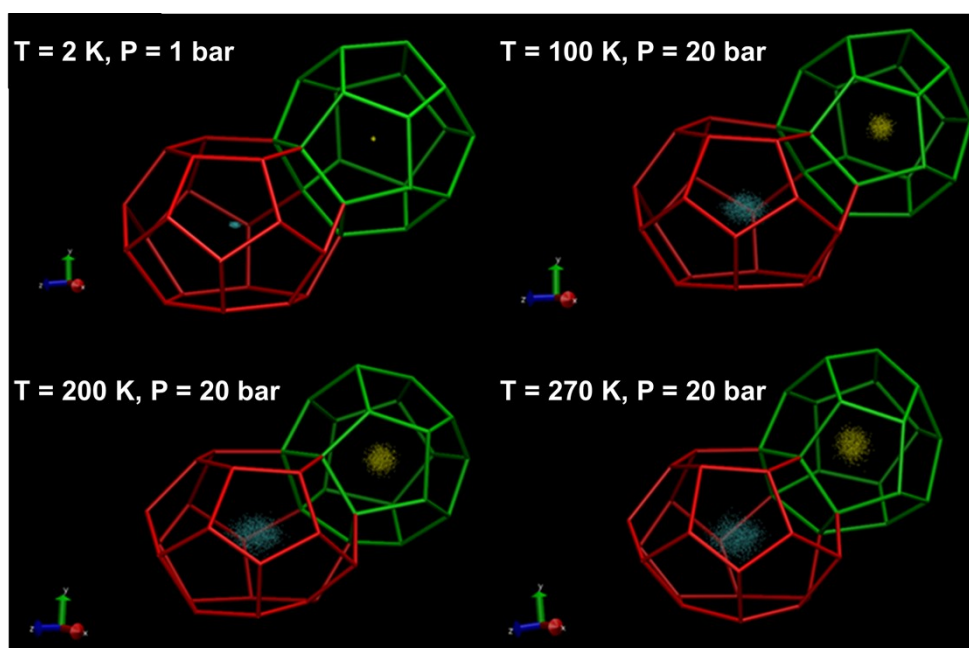
Figure S8. Typical structures of 5^{12} (green in color) and $5^{12}6^2$ (red in color) water-host cages, and the cumulated trajectory of methane molecules in the respective water-host cages, at different temperatures based on the MD simulations in this study.

Figure S8 provided further information on the displacement of guest methane molecules in the 5^{12} and $5^{12}6^2$ cages at different simulated temperatures. The relatively isotropic displacement of methane in the small 5^{12} water cages at all simulated temperatures was suggested. The displacement of methane in the $5^{12}6^2$ water cages was anisotropic, with favored movements along the direction parallel to the hexagonal water rings. At low temperatures, the displacements of guest molecules were within very small ranges, and the host water cages exhibited organized and rigid structures. The increased dynamics features in structures of water cages and displacements of guest molecules in **Figure S8** agreed well with the PDF results in **Figure S7**.
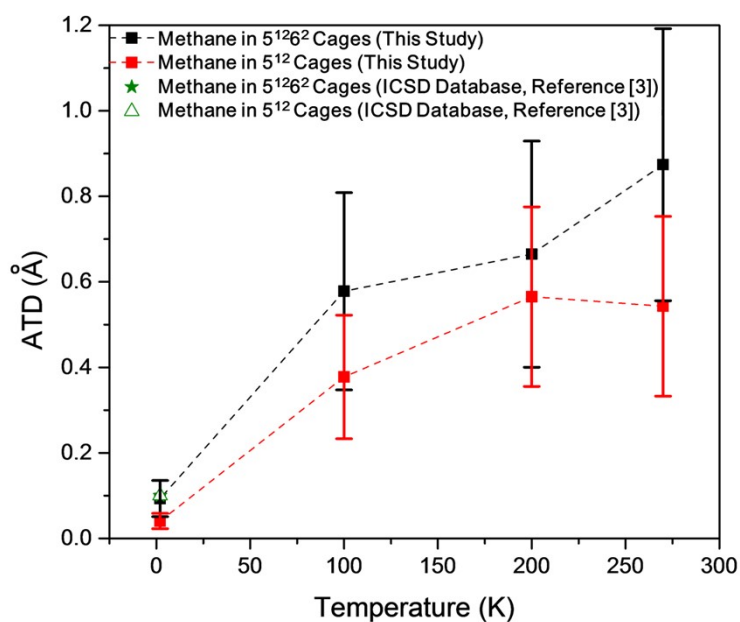
Figure S9. Atomic displacement (*i.e.* the mean square displacement) of methane molecules in the 5^{12} and $5^{12}6^2$ water host cages (values averaged from the MD simulations of 2 ns) at different temperatures based on the MD simulation results in this study[3].

    Figure S9 summarized the atomic displacement of guest methane molecules based on the MD simulation results at different temperatures, supplementary to **Figure S8**. Although continuous atomic displacement increase of guest methane in the $5^{12}6^2$ big water cages was suggested, the displacement of guest methane in the 5^{12} small water cages did not increase further, which was related to the intrinsic geometry limitations of the small water cages in Structure-I gas hydrates[3].

3.2 MD Simulations of the Configurations with "MH - vacuum" and "MH - gas" Interfaces
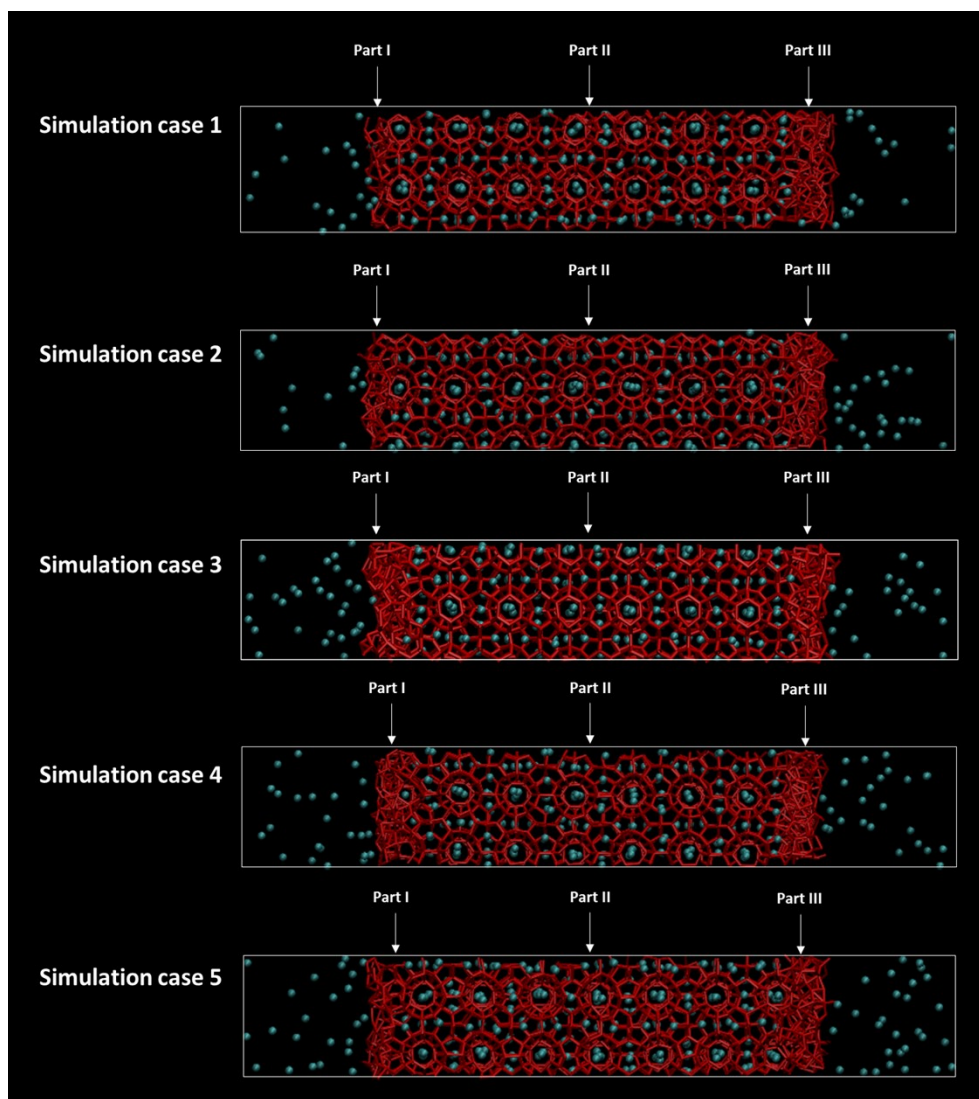
Figure S10. Snap-shots representing the configuration of different simulation cases at t = 50 ns (see also Figure 7 and Table 2). (Cyan: methane molecules, Red: hydrogen bonds formed by O – O atoms.)
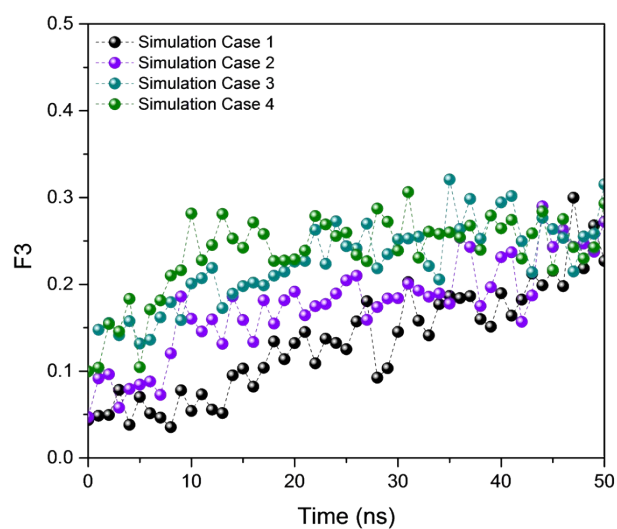
Figure S11. Typical evolutions of the F_3 parameter of the decomposed water molecules for simulation cases 1-4 (Table 2). (See also Figure S10; F3 parameter of simulation case 5 illustrated in Figure 8a).
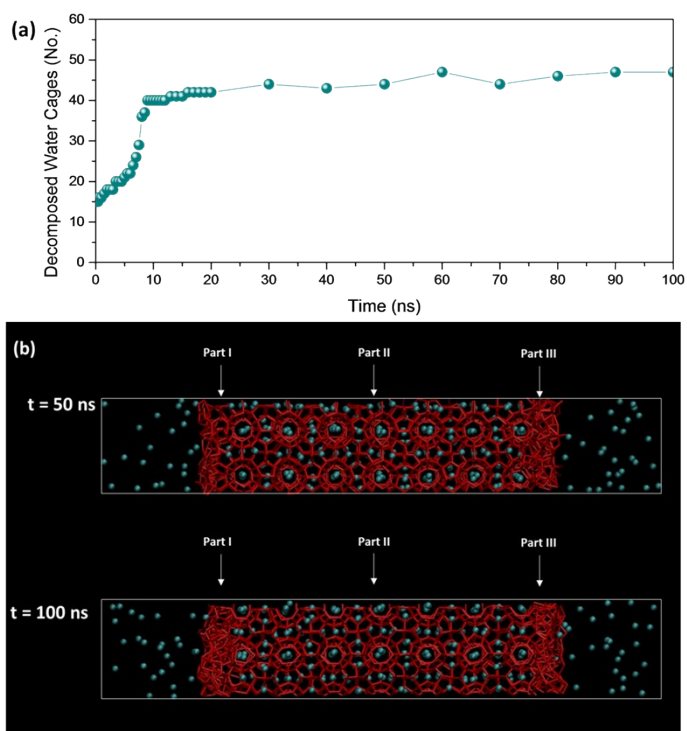
FigureS12. (a) The number of decomposed water cages for simulation case 5 with an extended simulation time to 100 ns, and **(b)** The corresponding snapshot at 100 ns compared to that at 50 ns.

References

1.	J. D. Lee, R. Susilo and P. Englezos, *Chemical Engineering Science*, 2005, **60**, 4203-4212.
2.	L. Jensen, *Experimental investigation and molecular simulation of gas hydrates*, Technical University of Denmark, 2010.
3.	C. Gutt, B. Asmussen, W. Press, M. Johnson, Y. Handa and J. Tse, *The journal of chemical physics*, 2000, **113**, 4713-4721.
4.	M. T. Kirchner, R. Boese, W. E. Billups and L. R. Norman, *Journal of the American Chemical Society*, 2004, **126**, 9407-9412.
5.	V. R. Belosludov, T. M. Inerbaev, O. S. Subbotin, R. V. Belosludov, J.-i. Kudoh and Y. Kawazoe, *Journal of Supramolecular Chemistry*, 2002, **2**, 453-458.
6.	S. Takeya, M. Kida, H. Minami, H. Sakagami, A. Hachikubo, N. Takahashi, H. Shoji, V. Soloviev, K. Wallmann and N. Biebow, *Chemical Engineering Science*, 2006, **61**, 2670-2674.
7.	V. Petkov, *Characterization of Materials*, 2012, 1361-1372.